Finite Element Simulation Technique for Evaluation of Opening Stresses Under High Plasticity

Ans Al Rashid
Hamad Bin Khalifa University
Ramsha Imran
Institute of Space Technology
Muhammad Yasir Khalid (yasirkhalid94@gmail.com)
UNIVERSITY OF MANAGMENT AND TECHNOLOGY LAHORE https://orcid.org/0000-0002-4462-7951

Original Article

Keywords: Railway Steels, Fatigue Crack Closure, Simulation, Finite Element Analysis, Low Cycle Fatigue

Posted Date: November 25th, 2020

DOI: https://doi.org/10.21203/rs.3.rs-113059/v1

Finite element simulation technique for evaluation of opening stresses under high plasticity

Ans Al Rashid[1], Ramsha Imran[1], Muhammad Yasir Khalid[2*]

[1] Division of Sustainable Development, College of Science and Engineering, Hamad Bin Khalifa University, Qatar Foundation, Doha, Qatar
[2] Department of Mechanical Engineering, University of Management & Technology Lahore, Sialkot Campus, Pakistan
*Corresponding author: Muhammad Yasir Khalid (yasirkhalid94@gmail.com)

Abstract

The mechanical behavior of materials plays a vital role in the structural performance of designed structures. Therefore, significant resources are devoted globally towards experimental characterization of material behavior, especially for the experiments requiring particular protocols. Contrary, finite element analysis tools have made a substantial contribution to the design of structural elements, which could conserve a significant amount of resources and material wastage. Evaluation of fatigue life of materials is necessary to predict the life expectancy of the structures precisely, and opening stress levels under fatigue loading contributes towards this evaluation. Railways serve as freight and passenger carrier transportation modes. The railway axles contribute as the primary load-carrying element; therefore, the design of railway axles and the study of their mechanical behavior under repeated loading is vital. In this study, the authors present a finite element simulation technique to evaluate the opening stress levels for two structural steels subjected to low cycle fatigue. The finite element analysis (FEA) model was designed and validated following the simulation of fatigue crack propagation under high plasticity conditions. Numerical simulation results were compared with the experimental results obtained earlier through the digital image correlation (DIC) technique. To conclude, FEA could be a useful tool to predict crack closure phenomena and, ultimately, the fatigue life of components. However, researchers

need to establish more sophisticated numerical tools for more precise results in case of high plasticity conditions near the crack tip.

Keywords: Railway Steels; Fatigue Crack Closure; Simulation; Finite Element Analysis; Low Cycle Fatigue.

1. Introduction

Railways serve as actual freight and passenger carrier transportation modes. The railway axles contribute as the primary load-carrying element; therefore, the design of railway axles and the study of their mechanical behavior under repeated loading is vital. The safe and reliable design of railway axles is indispensable to assure the safety of vehicles and passengers. Generally, for evaluation of fatigue life components undergoing high cycle fatigue are characterized under an infinite life standard. However, the fatigue life cannot be determined for parts experiencing low cycle fatigue (LCF) using this approach due to high plastic deformations involved.

In recent years, the interest in the study of fatigue strength of railway axles has significantly increased [1]–[4]. The crack opening load is mostly determined under both low and high cycle fatigue by various experimental techniques [5]–[9] and numerical methods [10]–[14]. In the case of complexities, Finite element analysis (FEA) is a prime choice over an experimental approach. Now FEA is widely used successfully predicting opening and closure stress [15].

Newman [16], for the very first time, simulated the finite element crack closure simulation. Under low nominal stress level, fine mesh size was beneficial for convergence, but element size can be relaxed when higher loads were applied. The problem in simulating the fatigue crack in FEA is relatively large discrete jumps corresponding to one element in front of the crack tip. Several

methods in literature present about when to release the node in a loading cycle and when to measure the closure levels after node release.

Pommier and Bompard [17] performed the FEA simulation of crack growth using Chaboche Plasticity Model with Von Mises Yield Criterion. The authors conducted the computations under plane strain conditions using the node release scheme to release the node at maximum strain amplitude. Two cycles per crack length were simulated, and opening levels were determined at the second cycle for each crack length. Crack was considered to be open when the displacement of the second node behind the crack tip reached 1.5% of its maximum value.

Now researchers are trying to incorporate XFEM in combination with the visco-plastic constitutive model, which is the high-temperature plasticity model with Z and n as a visco-plastic parameter along with Chaboche model parameters [18]. Simulations were performed in ABAQUS with strain accumulation criteria for crack growth. The predicted crack growth rate using XFEM was in comparison with experimental crack growth.

In another study, full-field characterization was performed on stainless steel 316L near-tip deformation for growing cracks under cyclic loading conditions. Results from both FEA and digital image correlation (DIC) revealed that crack closure was present during stable fatigue crack growth from crack opening displacement (COD) measurement [19].

Fatigue crack closure in AISI 304 stainless steel was studied experimentally and numerically [20]. The size of finite elements in the numerical model controlled the illustration of macro-changes in a rough crack profile. Results revealed that surface roughness caused a mismatch of the crack faces and to the uneven distribution of surface contact forces at the cycle minimum.

Y. Song et al. [21] studied the low cycle fatigue behavior of AH-32 steel through both experimental and numerical techniques. The crack closure level was measured under different load variations. The results revealed that a strong correlation existed between low cycle fatigue (LCF) and magnitude stress.

H. Alizadeh et al. [22] compared the results of two- and three-dimensional plane stress and strain FEA for prediction of crack opening in center cracked plate. A good match was observed between the plane stress finite element and actual strip applied stress levels for fine meshes.

Dong Qin et al. [23] conducted an LCF crack propagation experiment on Q345 steel. The results from the experiment and elastic-plastic finite element stress-strain analysis were compared under the different stress ratios. The authors found a good match between these techniques, and also crack closure phenomenon can be observed in a small region behind the crack tip. F.V. Antunes et al. [24] successfully performed numerical analysis on crack tip opening displacement (CTOD) of two different aluminum alloys and found a good relationship between da/dN and plastic CTOD.

Plasticity induced cracks drive crack closure phenomena under low cycle fatigue loading. However, very few publications are found in the literature addressing the finite element simulations of crack closure under high plasticity/low cycle fatigue conditions. The reported study, for the first time, presents the use of virtual extensometers to evaluate opening stress levels from FEA. In this study, numerical simulation of plasticity induced fatigue crack growth was performed using the Chaboche plasticity model, and results were compared to experimentally obtained opening stress levels using DIC presented in another study conducted by authors [25].

2. Materials and Methods

The material model was defined, which assisted in the simulation of material behavior. The crack propagation was simulated after the identification of material model parameters, and crack closure was observed using the finite element method (FEM). Obtained results were compared with experimental results from digital image correlation analysis reported in a previous study [25].

2.1. Low Cycle Fatigue (LCF) Tests

LCF experiments were performed on specimens without pre-crack to obtain the material parameters. Figure 1 presents the geometry of the sample. All the tests were performed regarding standard ASTM E 60692 (Standard Practice for Strain-Controlled Fatigue Testing) [26]. All the LCF experiments were conducted on the MTS-810 servo-hydraulic testing machine capable of applying a load up to 100 kN. Two types of structural steel were tested (30NiCrMoV12 and 25CrMo4).

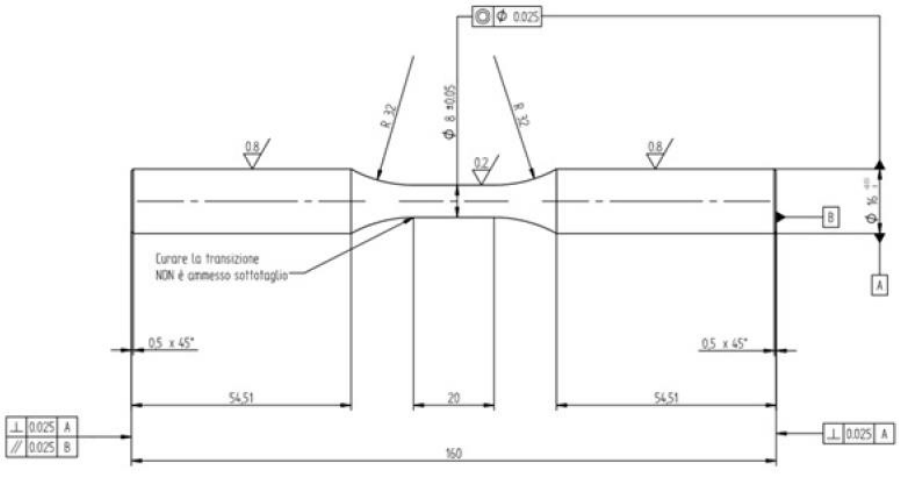

Figure 1. The geometry of Specimen for LCF Tests

2.2. Kinematic Hardening Model (Chaboche Model)

Ferrous materials exhibit some aspects of both kinematic and isotropic hardening until they become cyclically stable. After stabilization, they reveal only kinematic hardening. If transient

behavior is not of interest, a cyclically-stable material is assumed, and only kinematic hardening models are used. The kinematic hardening component is defined to be a combination of a purely kinematic term, linear ziegler hardening law, and a relaxation term which introduces non-linearity.

$$d\underline{\alpha} = \frac{2}{3} C d\underline{\varepsilon}^p - \gamma \underline{\alpha} dp \tag{1}$$

where, $\underline{\alpha}$= backstress vector; dp = equivalent plastic strain increment;

Integration of the back stress evolution laws for a uniaxial loading yields the expression:

$$\sigma - \sigma_0 = \frac{C}{\gamma}\left(1 - e^{-\gamma(\varepsilon_p - \varepsilon_p^0)}\right) + (\sigma_1 - \sigma_0) e^{-\gamma(\varepsilon_p - \varepsilon_p^0)} \tag{2}$$

Besides, several kinematic hardening components can be superimposed, which may considerably improve results in some cases. Typically, the use of 3 backstress vectors is enough for good modeling of the mechanical behavior of the material. Each kinematic term is expressed as:

$$d\underline{\alpha}^k = \frac{2}{3} C_k d\underline{\varepsilon}^p - \gamma_k \underline{\alpha}^k dp \tag{3}$$

Overall, backstress is the summation of individual backstress vectors.

$$\underline{\alpha} = \sum_{i=1}^{N} \underline{\alpha}^k \tag{4}$$

The kinematic hardening behavior of material was modeled using the above model.

2.2.1. Kinematic hardening parameters (30NiCrMoV12)

In total, 14 tests were performed on the material, 30NiCrMoV12, at three different strain ranges. All the tests were performed at load ratio ($R_\varepsilon = -1$), and the strain-ranges, as reported in Table 1. Kinematic hardening parameters were calculated using the Chaboche model with three backstress

115 vectors. Table 1 reports kinematic hardening parameters, and Figure 2 presents curve fitting for all
116 the samples.

117 **Table 1.** Material Parameters for 30NiCrMoV12

Strain Amplitude	C_1	C_2	C_3	γ_1	γ_2	γ_3
0.35%	704873.5	239478.5	1000	5000	350	0.01
0.50%	838792.6	125855.3	1000	5000	350	0.01
0.80%	844164.8	100441.7	1000	5000	350	0.01
Average	795943.7	155258.5	1000	5000	350	0.01

118

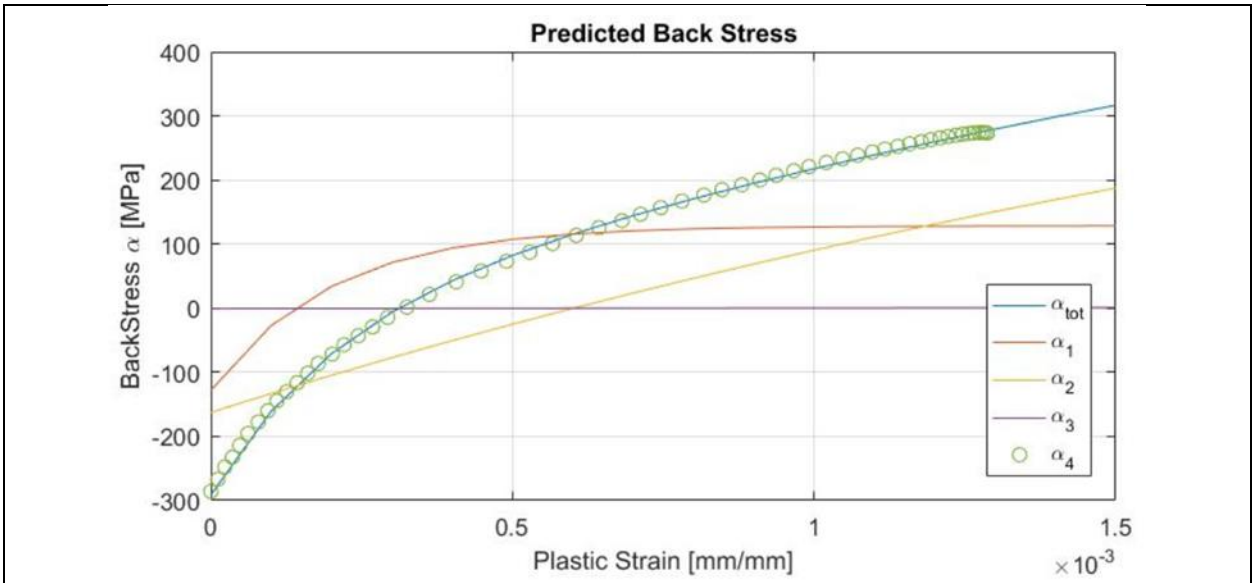

(a) Curve Fitting for 0.35% Strain Amplitude

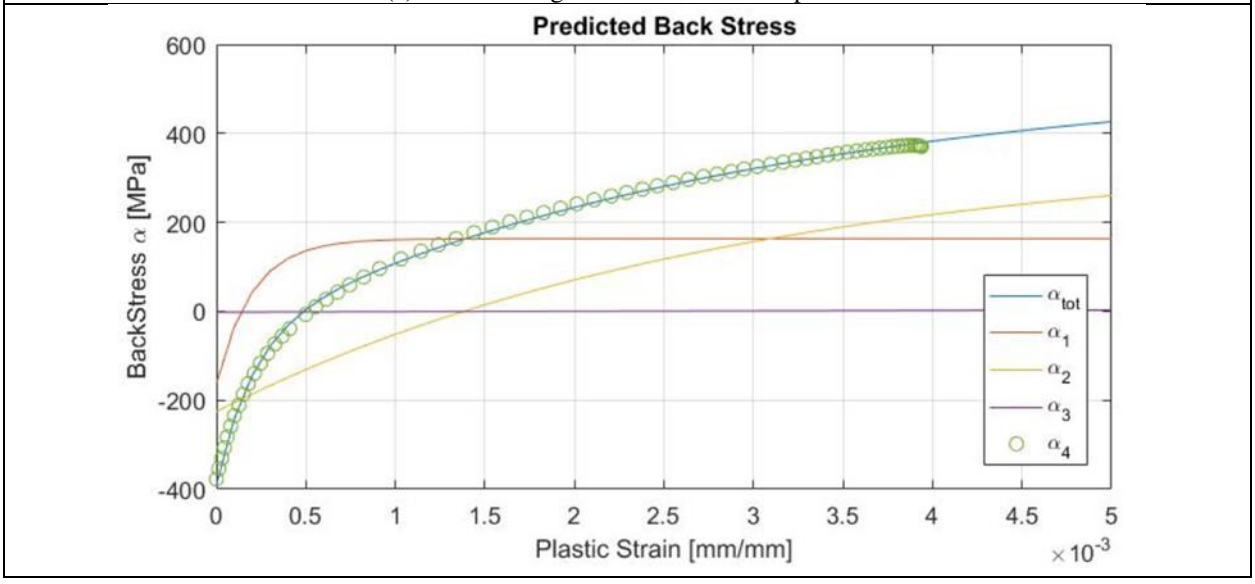

(b) Curve Fitting for 0.50% Strain Amplitude

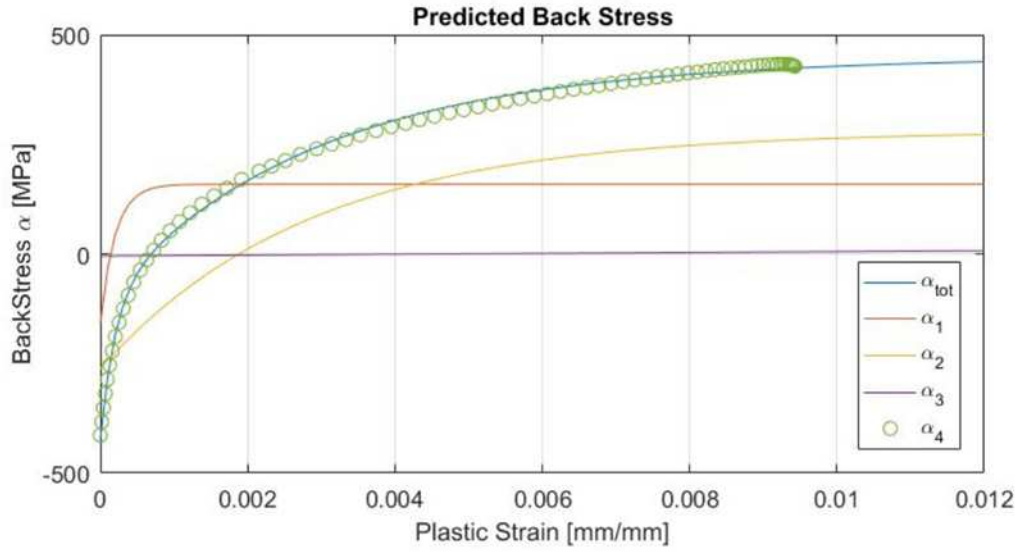

(c) Curve Fitting for 0.80% Strain Amplitude Test

Figure 2. Kinematic Hardening Model for 30NiCrMoV12

2.2.2. Kinematic hardening parameters (25CrMo4)

For identification of kinematic hardening parameters for 25CrMo4, six tests were performed on the material with the same specimen geometry used for 30NiCrMoV12 Steel at Strain Ratio ($R_\varepsilon = -1$) and strain amplitudes ($\varepsilon_{a1} = 0.60\%, \varepsilon_{a2} = 1.0\%, \varepsilon_{a3} = 1.50\%$). Table 2 presents the material parameters identified using the Chaboche model, and Figure 3 illustrates curve fitting at three strain amplitudes.

Table 2. Material Parameters for 25CrMo4

Strain Amplitude	C_1	C_2	C_3	γ_1	γ_2	γ_3
0.60%	356741.1	42579.45	1000	2500	250	0.01
1.00%	345933.3	40875.45	1000	2500	250	0.01
1.50%	392162.5	42689.25	1000	2500	250	0.01
Average	364945.6	42048.1	1000	2500	250	0.01

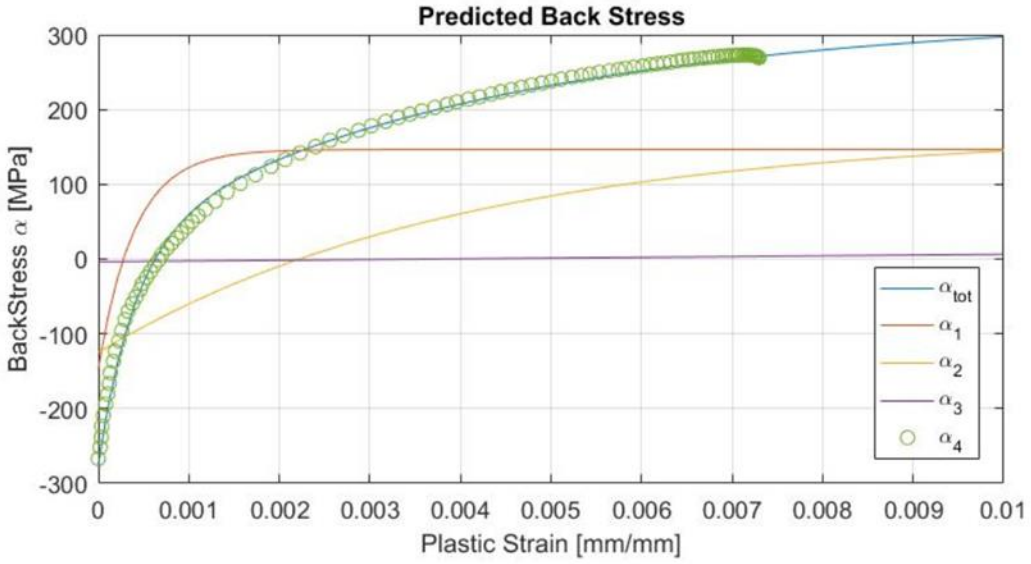

(a) Curve Fitting for 0.60% Strain Amplitude Test

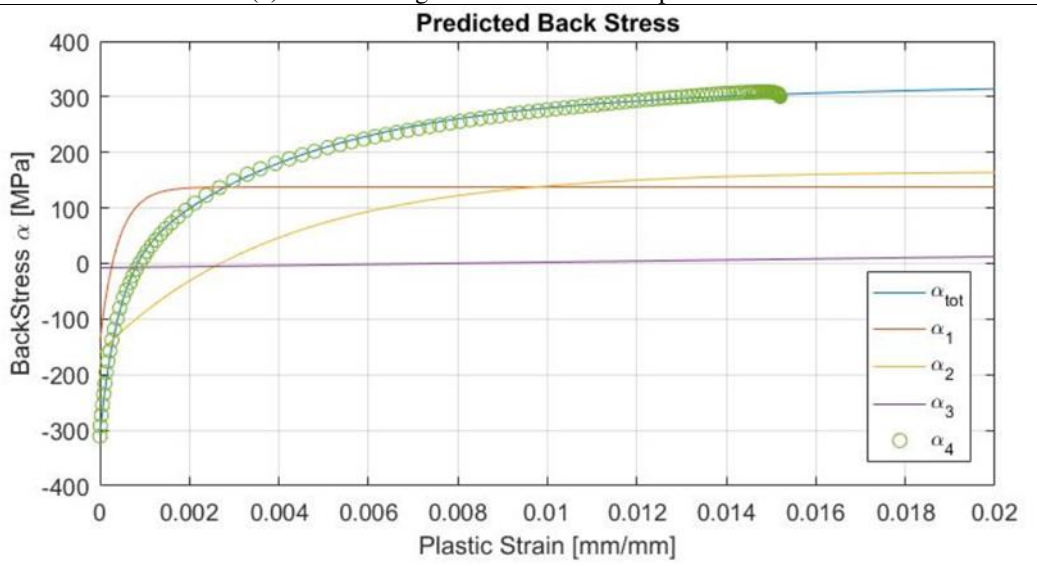

(b) Curve Fitting for 1.0% Strain Amplitude Test

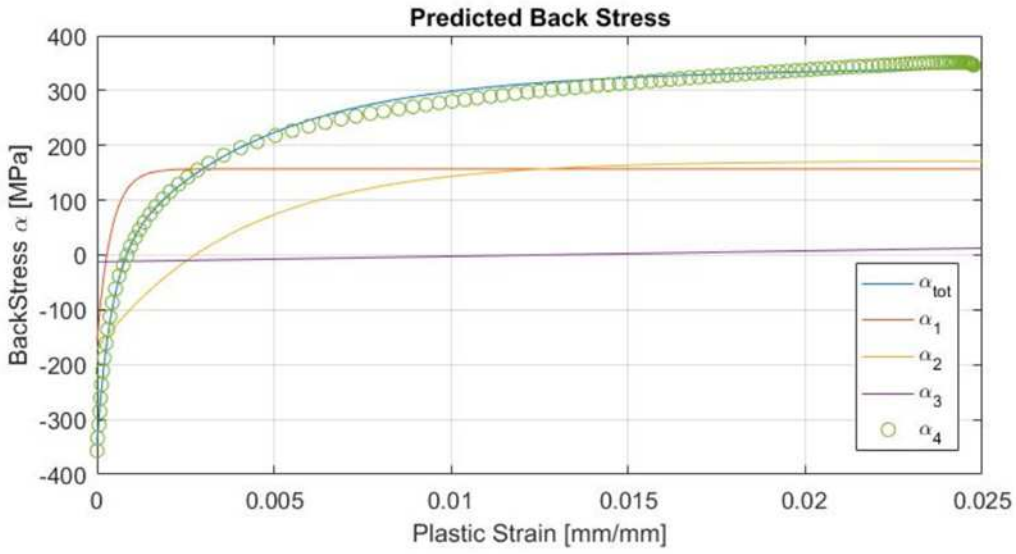

(c) Curve Fitting for 1.5% Strain Amplitude Test

Figure 3. Kinematic Hardening Model for 25CrMo4

2.3. Validation of Material Model

For the validation of material parameters, a cube of material (dimension 1mm x 1mm x 1mm) (as shown in Figure 4) was simulated to compare the bulk material behavior with experimental hysteresis loops. Modeled cube in FEA was assigned with material properties obtained from backstress fitting at different strain amplitudes. Stress/strain data was acquired from the visualization module of ABAQUS, and the same procedure was performed for all the strain amplitudes.

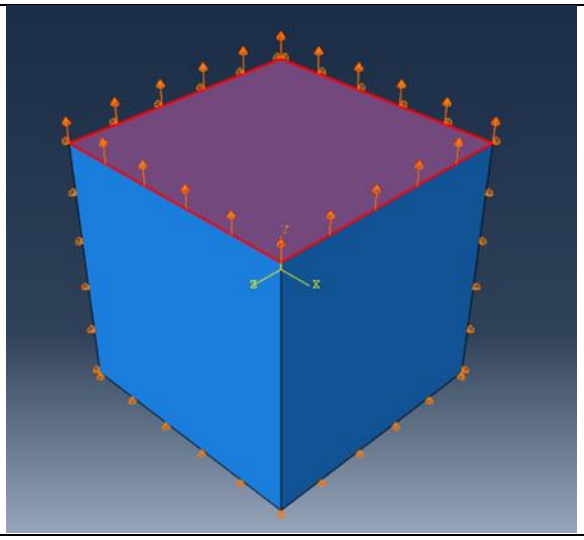

Figure 4. FEA Model for Material Model Validation

2.4. Fatigue Crack Simulation

After the identification and validation of material parameters, FEM simulation of a cracked plate was performed. The model can account for kinematic hardening of the material, and we are interested only in stabilized behavior. Both materials (30NiCrMoV12 and 25CrMo4) were simulated for crack closure observations.

Considering the symmetry of the specimen used for the determination of opening stresses using the DIC setup, only one-quarter of the plate was modeled, so plane stress conditions were assumed. The geometry of the plate modeled in ABAQUS is shown in Figure 5, along with dimensions of the plate. The crack growth was simulated using node release techniques [10]. During cycling of the material, one node was released after every three cycles, to stabilize the crack opening displacement in front of the crack tip. The dimensions of the plate were 7.0mm x 34.5mm. As simulated, a surface crack, symmetry about the x-axis was applied to the left edge of the plate, and vertical displacement was constrained for the bottom edge, Figure 5. A rigid surface was used to model the one-quarter of the specimen. Mesh size was refined along the crack axis, and the element

size was selected to be $20\mu m$. The crack grows from a pre-crack of $200-800\mu m$ which was the final crack length.

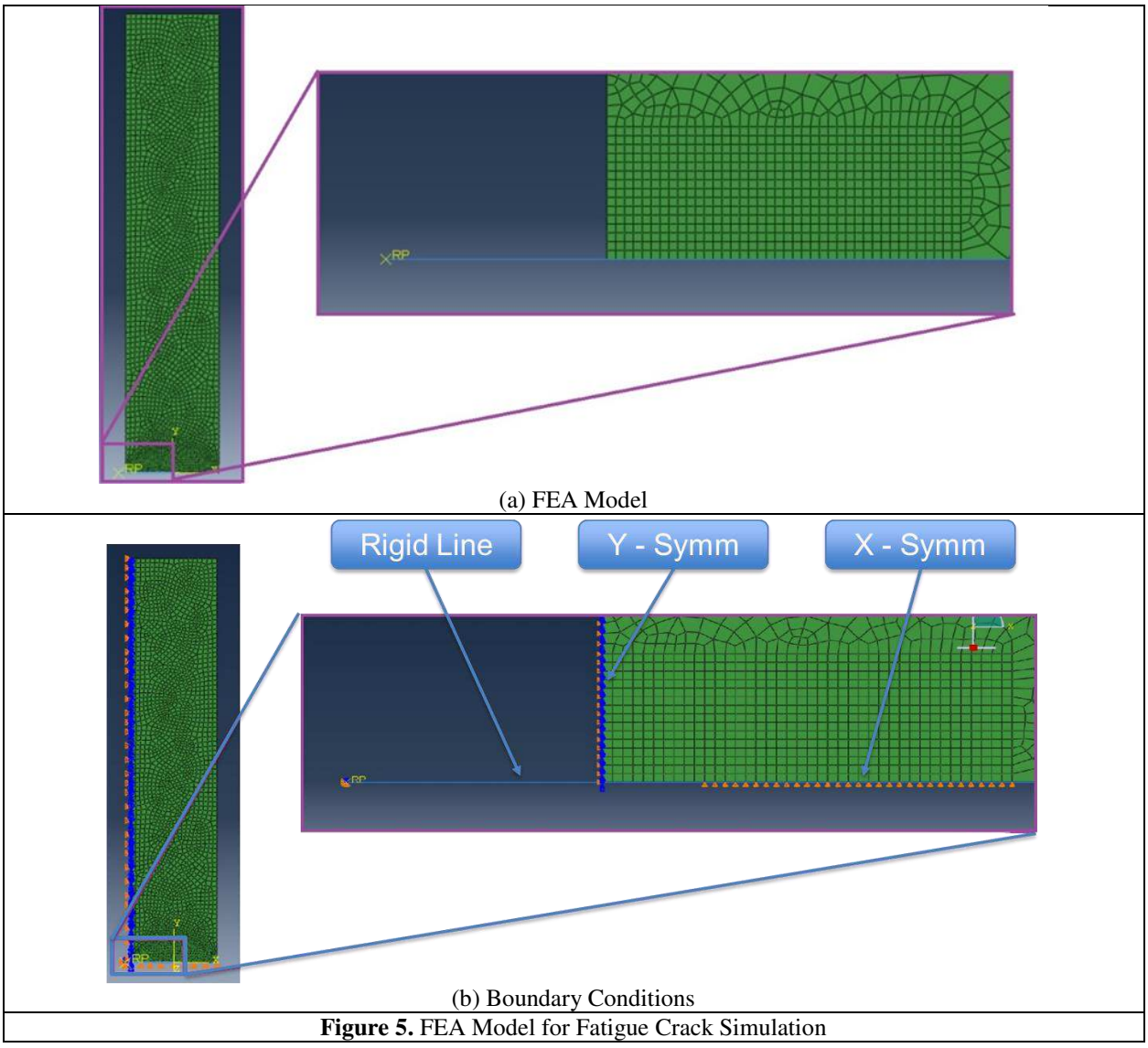

Figure 5. FEA Model for Fatigue Crack Simulation

2.5. Determination of Opening Stresses

For the determination of opening stresses, a relatively new approach was used. For a final crack length of $800\mu m$ a virtual extensometer was assumed to be placed various positions behind the crack tip (Figure 6). The size of an extensometer was taken constant $160\mu m$ and was consistent

159 with the virtual extensometer width used for DIC analysis. Each extensometer vertical
160 displacements were recorded during one loading cycle and plotted along with the stresses in far-
161 field. Then, removing the elastic part, a 1.5% Offset method was implemented for the
162 determination of opening levels. First, the stress vs. strain in far-field was compared with the
163 experimental results we had for the same strain range we were simulating. A comparison between
164 both is shown in Figure 7.

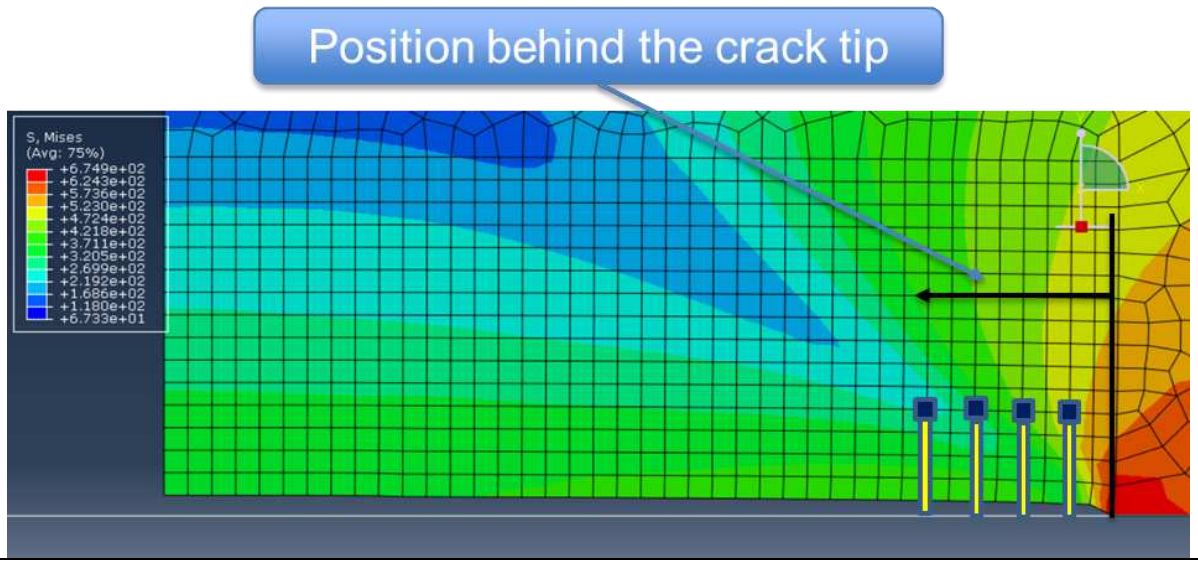

Figure 6. The positioning of the probe to obtain COD behind the Crack Tip

165

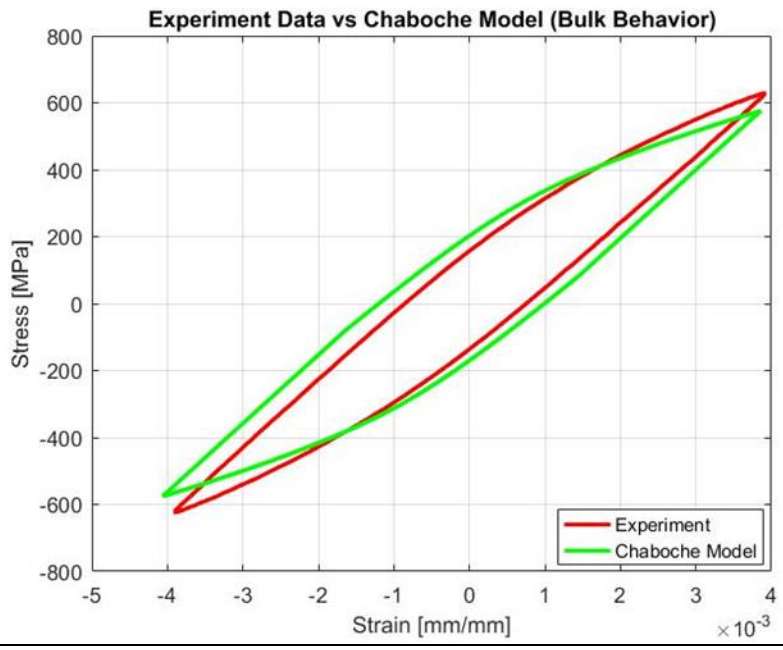

Figure 7. Bulk material behavior

166

167 Formerly, for different positions behind the crack tip and different crack lengths. Opening stresses
168 were calculated using the methodology defined. Vertical displacement data for one cycle was
169 extracted out at different positions behind the crack tip. After removing the elastic deformation
170 involved due to bulk material between the crack and the extensometer, a 1.5% Offset method was
171 employed for the determination of opening stresses (Figure 8).

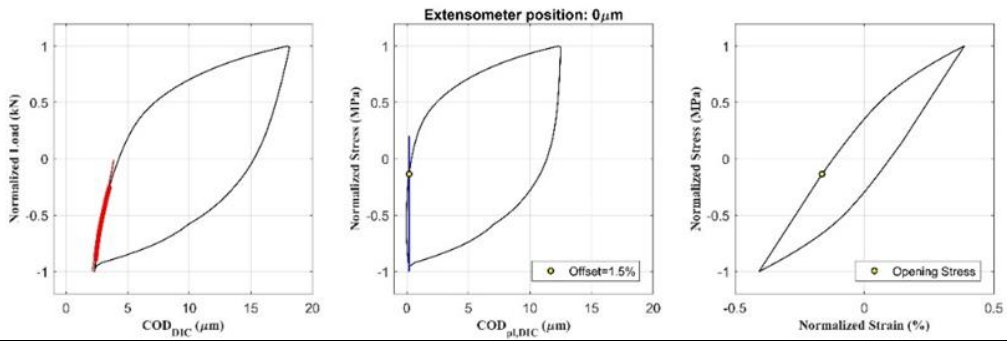

Figure 8. Determination of Opening Stresses (Crack 1600µm, 30NiCrMoV12, $\Delta\varepsilon$ = 0.80%)

172

Likewise, opening stresses for different crack lengths were obtained. Opening stresses values were observed to be stable along with the extensometer position behind the crack tip. Opening stress values along the crack are plotted in Figure 9.

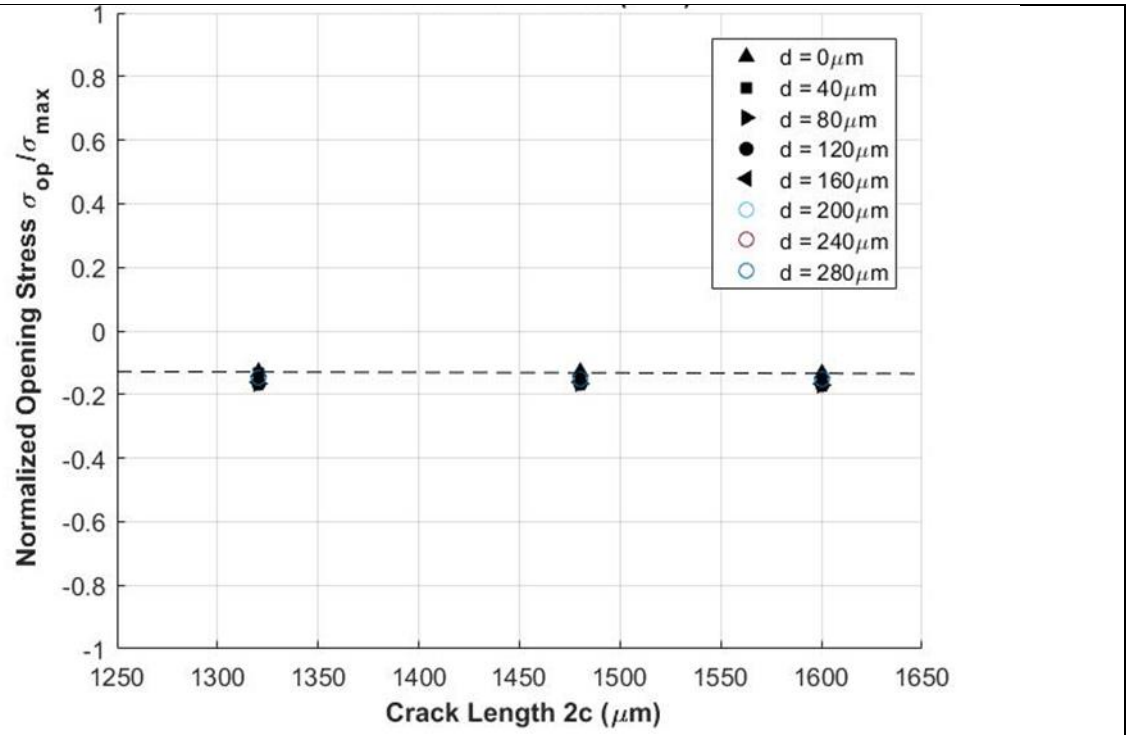

Figure 9. Crack Length vs Normalized Opening Stresses (FEM), 30NiCrMoV12, $\Delta\varepsilon = 0.80\%$

Likewise, finite element simulations were performed for 30NiCrMoV12 and 25CrMo4 for the strain amplitudes tested during the experiments, and different strain ranges for 25CrMo4.

3. Results and Discussion

3.1. Material Model

After simulating three strain ratios, at which material was tested during DIC experiments, the stabilized hysteresis loops were compared with experimental results. The comparison between ABAQUS analysis and experimental results of the three strain amplitudes are reported in Figure 10.

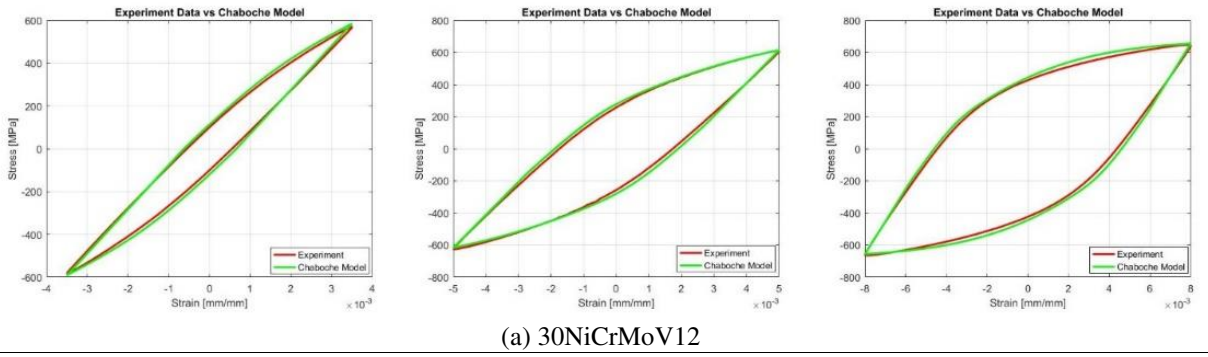

(a) 30NiCrMoV12

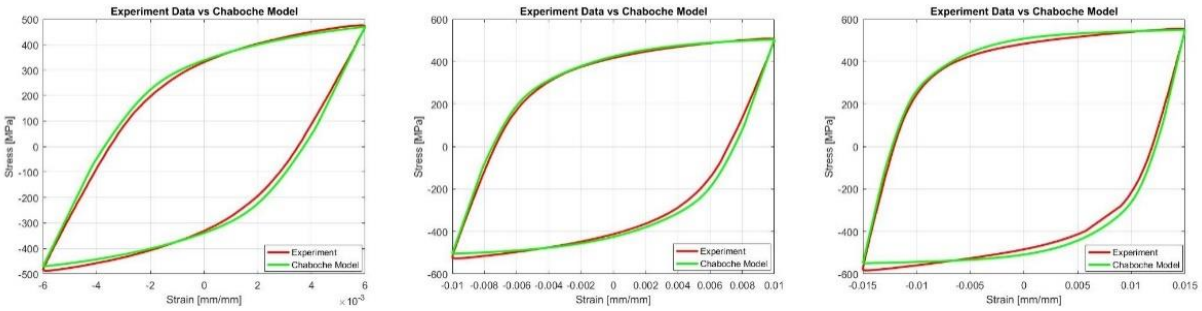

(b) 25CrMo4

Figure 10. Material Model vs. Experiments

185

186 If we use averaged parameters for simulation of the same strain amplitudes, then these parameters
187 do not agree very well with the experimental results for 30NiCrMoV12 but the perfect prediction
188 for 25CrMo4 steel even with the use of averaged parameters, as shown in Figure 11.

189

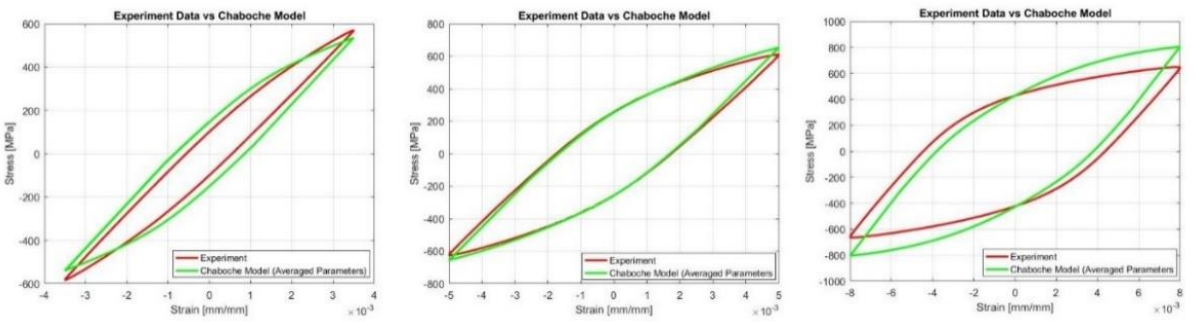

(a) 30NiCrMoV12

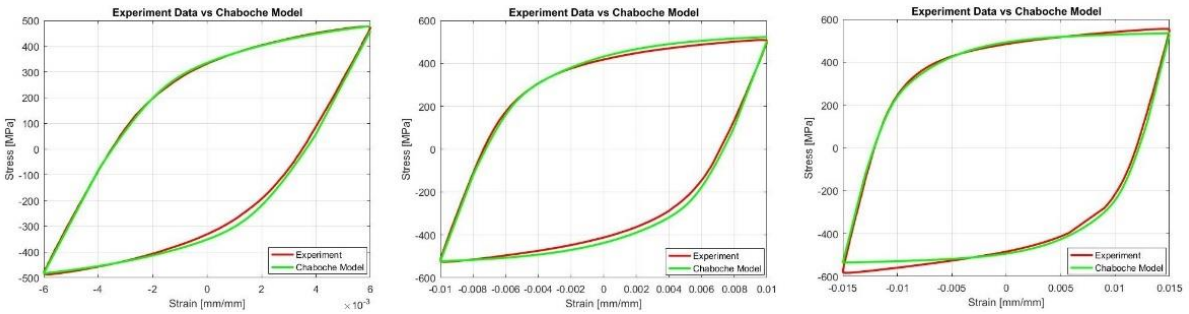

(b) 25CrMo4

Figure 11. Material Model (Averaged Parameters) vs. Experiments

190

191 **3.2. Fatigue Crack Simulation**

192 FEM crack propagation simulation was performed at 0.3%, 0.4%, and 0.5% strain amplitude, and
193 the opening stresses from FEM were compared with the experimental results of 30NiCrMoV12
194 and 25CrMo4 tested at same strain range**.** The finite element model overestimates the opening
195 stress levels, while experimental analysis showed a lower level of opening stresses. For
196 30NiCrMoV12 tested at strain ratio -1, the FEM model provided results with reasonable accuracy.
197 However, for high strain rates, the discrepancy between results increases. For 25CrMo4, the FEM
198 model provided the same trends as obtained from experimental results for all the strain rates tested.
199 Figure 12.

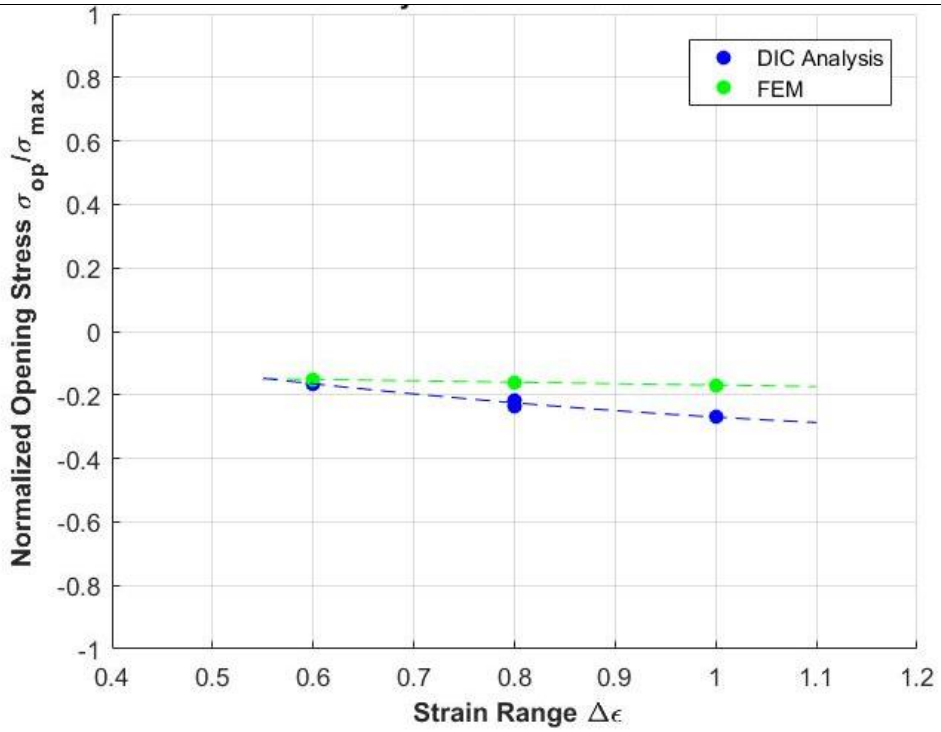

(a) σ_{op} vs $\Delta\varepsilon$ (30NiCrMoV12, R = -1)

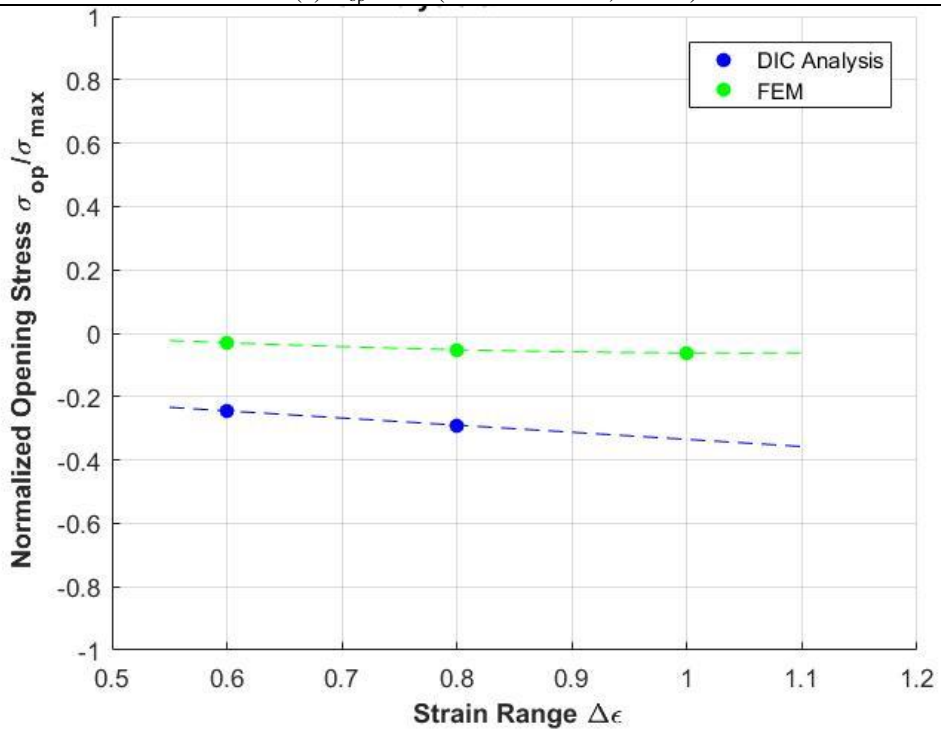

(b) σ_{op} vs $\Delta\varepsilon$ (25CrMo4, R = -1)

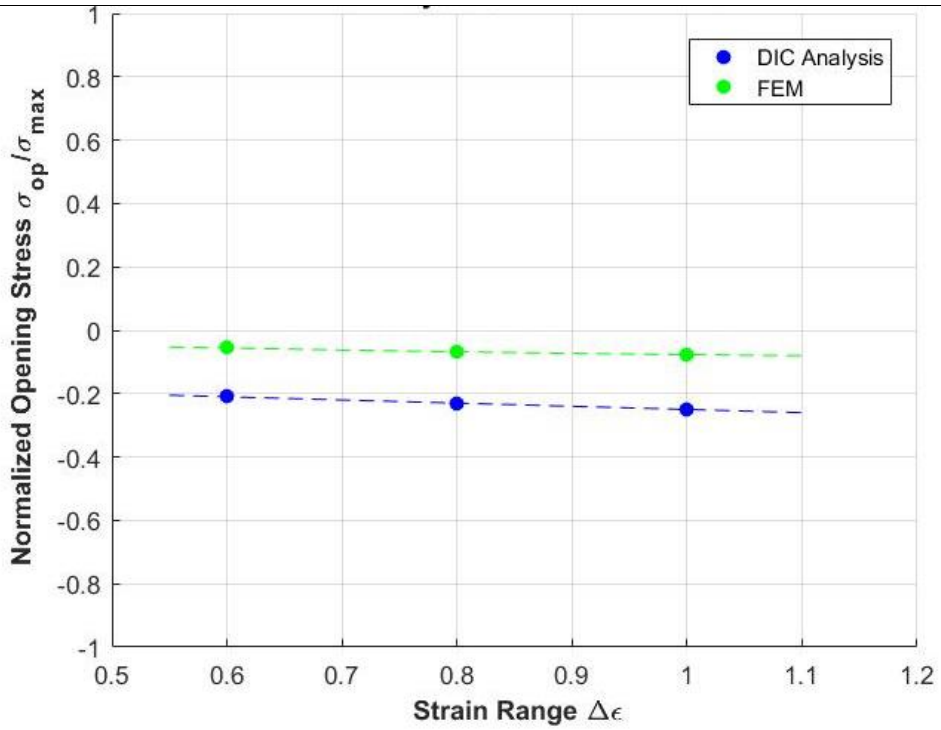

(c) σ_{op} vs $\Delta\varepsilon$ (25CrMo4, R = 0)

Figure 12. Opening Stresses Levels for different materials vs. Strain Ranges

FEM model overestimates the opening levels for all the strain ranges and strain amplitudes simulated. The discrepancy between experimental and numerical results was owed to two main reasons. First, the FEM model overestimates maximum COD value as compared to experimental results [25], and due to fixed offset value (1.5% of maximum COD value), opening levels are overestimated. Secondly, as mentioned in section 2.3, authors have used averaged parameters for fatigue crack simulation obtained at different strain rates. But due to high plastic strain accumulation near the crack tip model interpolates the strain values from the parameters used for analysis. FEM (ABAQUS) allows only a single set of hardening parameters for material properties. However, plasticity accumulation at the crack tip and far-field properties (which are basically under elastic region) require different material properties, that's the limitation of FEM. It is worth mentioning that for 30NiCrMoV12, the FEM model provided an excellent agreement with DIC

213 analysis results and strengthens the above argument. Also, a surface crack was considered, which
214 was a simplified model of 3D-crack. Another factor is the simulation of the only plasticity induced
215 crack, which is horizontal, but the crack is not horizontal all the time, and roughness was also
216 ignored along the crack flanks to simplify the model.

217 **4. Conclusions**

218 In this study, an evaluation of opening stresses for railway steels (25CrMo4 and 30NiCrMoV12)
219 subjected to LCF was performed using finite element analysis. The concept of crack opening
220 displacement (COD) was used for the study. Numerical simulation results were compared with the
221 experimental results obtained earlier using digital image correlation (DIC) technique [25].

222 Opening stresses were successfully evaluated using FEA tools, but there existed some errors which
223 were caused by limitations of the means used. The simple 2D model is used to simulate crack
224 propagation in FEM. FEM model provides a reasonable estimation of the opening stresses. A
225 similar trend can be observed if compared to experimental results, that opening stresses decreases
226 with an increase in strain amplitude. But the model overestimates the opening levels; it is because
227 the model is assigned with the averaged material properties obtained from different strain
228 amplitude LCF tests. Secondly, a surface crack was considered, which was a simplified model of
229 3D-crack. Another factor is the simulation of the only plasticity induced crack, which is horizontal,
230 but the crack is not horizontal all the time, and roughness was also ignored along the crack flanks
231 to simplify the model. So, the model can't precisely predict openings at all the strain ranges.
232 However, it is concluded that finite element analysis (FEA) could be a useful tool to predict crack
233 closure phenomena and, ultimately, the fatigue life of components. However, more sophisticated
234 numerical tools need to be developed for more precise results in case of high plasticity conditions
235 near the crack tip.

Abbreviations

Finite element analysis (FEA)
low cycle fatigue (LCF)
digital image correlation (DIC)
crack opening displacement (COD)
crack tip opening displacement (CTOD)
Finite element method (FEM)

Availability of data and materials

Data will made available on request.

Funding

This research work did not receive any funding.

Competing Interest

The authors declare that they have no conflict of interest.

Authors' contributions

Conceptualization, A.A.R and M.Y.K.; methodology, R.I. and A.A.R.; validation, M.Y.K.;format analysis, R.I.; the investigation, M.Y.K and A.A.R.; writing—original draft preparation, M.Y.K.; writing—review & editing, R.I. and M.Y.K.; project administration, A.A.R. All authors have read and agreed to the published version of the manuscript

Acknowledgments

Experiments were performed at Mechanical Material Testing Lab, Mechanical Engineering Department, Politecnico Di Milano, Italy.

5. References

[1] J. Zhang, H. Li, B. Yang, B. Wu, and S. Zhu, “Fatigue properties and fatigue strength evaluation of railway axle steel: Effect of micro-shot peening and artificial defect,” *Int. J.*

Fatigue, vol. 132, p. 105379, 2020, doi: 10.1016/j.ijfatigue.2019.105379.

[2] S. Beretta, M. Carboni, G. Fiore, and A. Lo Conte, "Corrosion-fatigue of A1N railway axle steel exposed to rainwater," *Int. J. Fatigue*, vol. 32, no. 6, pp. 952–961, 2010, doi: 10.1016/j.ijfatigue.2009.08.003.

[3] J. Leander, A. Andersson, and R. Karoumi, "Monitoring and enhanced fatigue evaluation of a steel railway bridge," *Eng. Struct.*, vol. 32, no. 3, pp. 854–863, 2010, doi: 10.1016/j.engstruct.2009.12.011.

[4] Z. Liao *et al.*, "Short fatigue crack behaviour of LZ50 railway axle steel under multi-axial loading in low-cycle fatigue," *Int. J. Fatigue*, vol. 132, no. July, p. 105366, 2020, doi: 10.1016/j.ijfatigue.2019.105366.

[5] M. Benedetti, V. Fontanari, C. Santus, and M. Bandini, "Notch fatigue behaviour of shot peened high-strength aluminium alloys: Experiments and predictions using a critical distance method," *Int. J. Fatigue*, vol. 32, no. 10, pp. 1600–1611, 2010, doi: 10.1016/j.ijfatigue.2010.02.012.

[6] Y. S. Yang, K. J. Son, S. K. Cho, S. G. Hong, S. K. Kim, and K. H. Mo, "Effect of residual stress on fatigue strength of resistance spot weldment," *Sci. Technol. Weld. Join.*, vol. 6, no. 6, pp. 397–401, 2001, doi: 10.1179/stw.2001.6.6.397.

[7] Y. Garbatov, C. Guedes Soares, and J. Parunov, "Fatigue strength experiments of corroded small scale steel specimens," *Int. J. Fatigue*, vol. 59, pp. 137–144, 2014, doi: 10.1016/j.ijfatigue.2013.09.005.

[8] E. Troiano, A. P. Parker, J. Underwood, and C. Mossey, "Experimental data, numerical fit

and fatigue life calculations relating to the Bauschinger effect in high strength armament steels," *J. Press. Vessel Technol. Trans. ASME*, vol. 125, no. 3, pp. 330–334, 2003, doi: 10.1115/1.1593072.

[9] F. Yousefi, M. Witt, and H. Zenner, "Fatigue strength of welded joints under multiaxial loading: Experiments and calculations," *Fatigue Fract. Eng. Mater. Struct.*, vol. 24, no. 5, pp. 339–355, 2001, doi: 10.1046/j.1460-2695.2001.00397.x.

[10] D. Camas, J. Garcia-Manrique, F. Perez-Garcia, and A. Gonzalez-Herrera, "Numerical modelling of three-dimensional fatigue crack closure: Plastic wake simulation," *Int. J. Fatigue*, vol. 131, no. October, p. 105344, 2020, doi: 10.1016/j.ijfatigue.2019.105344.

[11] H. Ito, Y. Suzuki, H. Nishikawa, M. Kinefuchi, M. Enoki, and K. Shibanuma, "Multiscale model prediction of ferritic steel fatigue strength based on microstructural information, tensile properties, and loading conditions (no adjustable material constants)," *Int. J. Mech. Sci.*, vol. 170, no. July 2019, p. 105339, 2020, doi: 10.1016/j.ijmecsci.2019.105339.

[12] B. Marques, L. P. Borrego, J. M. Ferreira, F. V. Antunes, and R. Branco, "A numerical analysis of fatigue crack closure using CTOD," *Procedia Struct. Integr.*, vol. 18, pp. 645–650, 2019, doi: 10.1016/j.prostr.2019.08.211.

[13] R. C. McClung, "Finite Element Analysis of Specimen Geometry Effects on Fatigue Crack Closure," *Fatigue Fract. Eng. Mater. Struct.*, vol. 17, no. 8, pp. 861–872, 1994, doi: 10.1111/j.1460-2695.1994.tb00816.x.

[14] J. D. Skinner and S. R. Daniewicz, "Simulation of plasticity-induced fatigue crack closure in part-through cracked geometries using finite element analysis," *Eng. Fract. Mech.*, vol. 69, no. 1, pp. 1–11, 2001, doi: 10.1016/S0013-7944(01)00115-1.

[15] K. Solanki, S. R. Daniewicz, and J. C. Newman, “Finite element analysis of plasticity-induced fatigue crack closure: An overview,” *Eng. Fract. Mech.*, vol. 71, no. 2, pp. 149–171, 2004, doi: 10.1016/S0013-7944(03)00099-7.

[16] J. C. Newman, “A Finite-Element Analysis of Fatigue Crack Closure,” in *Mechanics of Crack Growth*, J. R. Rice and P. C. Paris, Eds. West Conshohocken, PA: ASTM International, 1976, pp. 281–301.

[17] S. POMMIER and P. BOMPARD, “Bauschinger effect of alloys and plasticity-induced crack closure: a finite element analysis,” *Fatigue Fract. Eng. Mater. Struct.*, vol. 23, no. 2, pp. 129–139, 2000.

[18] F. Farukh, L. Zhao, R. Jiang, P. Reed, D. Proprentner, and B. Shollock, “Fatigue crack growth in a nickel-based superalloy at elevated temperature - experimental studies, viscoplasticity modelling and XFEM predictions,” *Mech. Adv. Mater. Mod. Process.*, vol. 1, no. 1, pp. 1–13, 2015, doi: 10.1186/s40759-015-0003-4.

[19] S. Alshammrei, B. Lin, and J. Tong, “Full-field experimental and numerical characterisation of a growing fatigue crack in a stainless steel,” *Int. J. Fatigue*, vol. 133, no. August 2019, p. 105449, 2020, doi: 10.1016/j.ijfatigue.2019.105449.

[20] A. Materna, H. Lauschmann, and J. Ondráček, “Numerical Modelling of Plasticity Induced Crack Closure with Rough Fracture Surfaces,” *Key Eng. Mater.*, vol. 827, pp. 7–12, 2019, doi: 10.4028/www.scientific.net/kem.827.7.

[21] Y. Song, P. Yang, Z. Peng, and W. Jiang, “Low-Cycle Fatigue Crack Propagation Behavior of Cracked Steel Plates Considering Accumulative Plastic Strain,” *Int. J. Steel Struct.*, no. 1970, 2019, doi: 10.1007/s13296-019-00303-6.

[22] H. Alizadeh *et al.*, “A comparison of two and three-dimensional analyses of fatigue crack closure,” *Int. J. Fatigue*, vol. 29, no. 2, pp. 222–231, 2007, doi: 10.1016/j.ijfatigue.2006.03.014.

[23] Q. Dong, P. Yang, G. Xu, and J. Deng, “Mechanisms and modeling of low cycle fatigue crack propagation in a pressure vessel steel Q345,” *Int. J. Fatigue*, vol. 89, pp. 2–10, 2016, doi: 10.1016/j.ijfatigue.2016.03.026.

[24] F. V. Antunes, S. M. Rodrigues, R. Branco, and D. Camas, “A numerical analysis of CTOD in constant amplitude fatigue crack growth,” *Theor. Appl. Fract. Mech.*, vol. 85, pp. 45–55, 2016, doi: 10.1016/j.tafmec.2016.08.015.

[25] A. Al Rashid, R. Imran, and M. Y. Khalid, “Determination of opening stresses for railway steel under low cycle fatigue using digital image correlation,” *Theor. Appl. Fract. Mech.*, vol. 108, no. April, p. 102601, 2020, doi: 10.1016/j.tafmec.2020.102601.

[26] A. Standard, “E606-92,” *Stand. Pract. Strain-Controlled Fatigue Testing,” Annu. B. ASTM Stand.*, vol. 3, 2004.

Figures

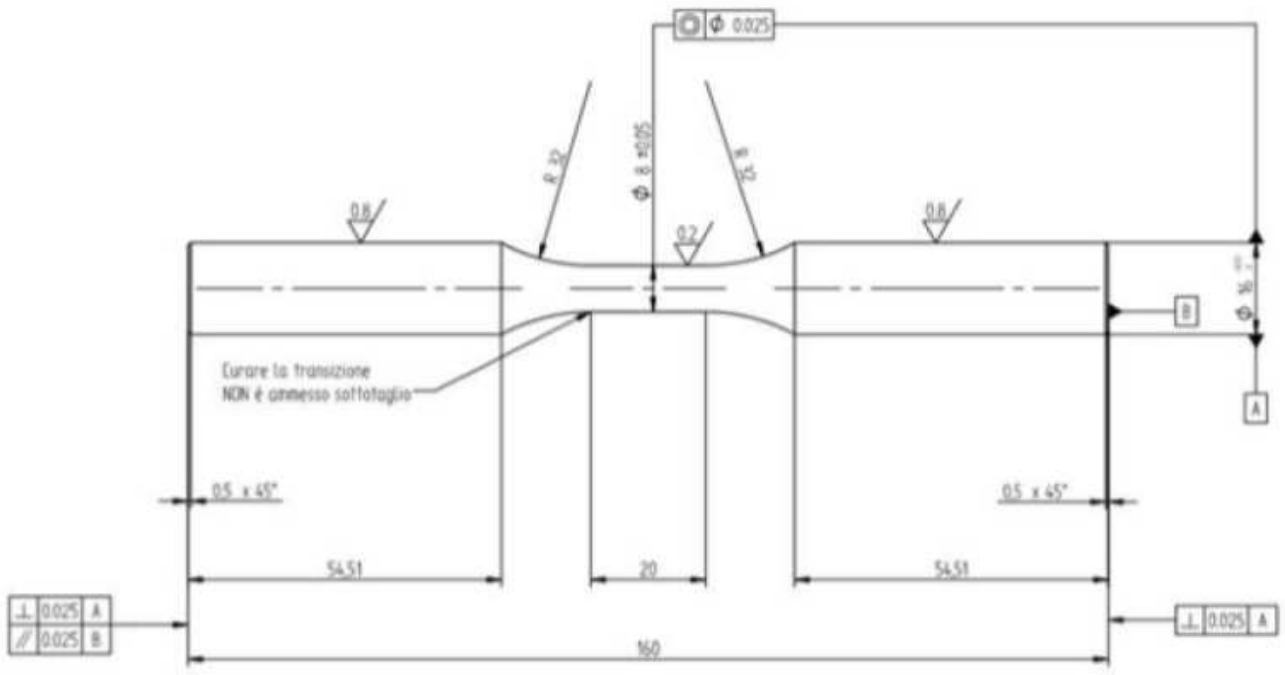

Figure 1

The geometry of Specimen for LCF Tests

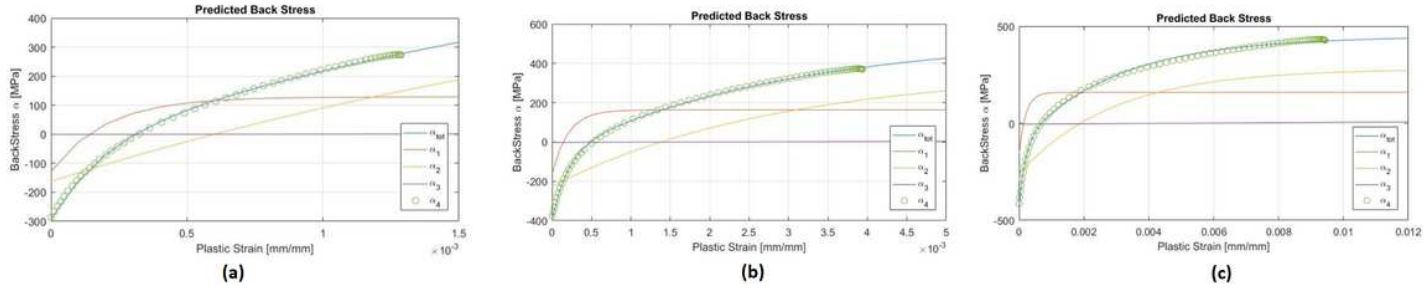

Figure 2

Kinematic Hardening Model for 30NiCrMoV12 (a) Curve Fitting for 0.35% Strain Amplitude (b) Curve Fitting for 0.50% Strain Amplitude (c) Curve Fitting for 0.80% Strain Amplitude Test

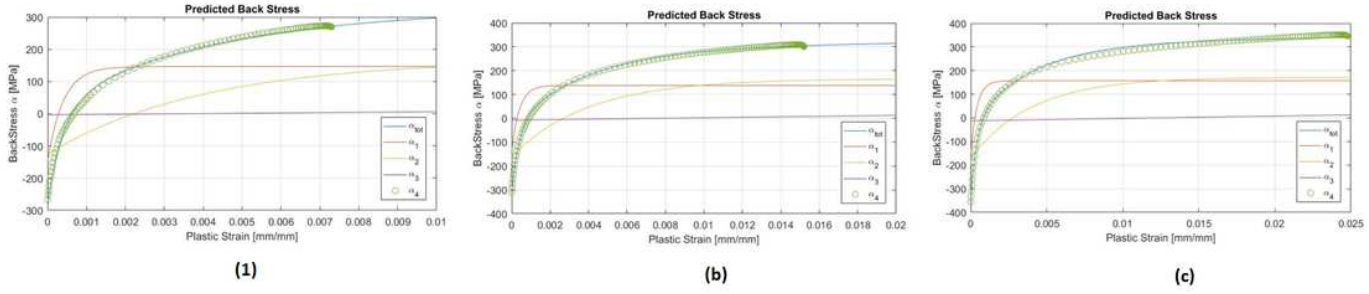

Figure 3

Kinematic Hardening Model for 25CrMo4 (a) Curve Fitting for 0.60% Strain Amplitude Test (b) Curve Fitting for 1.0% Strain Amplitude Test (c) Curve Fitting for 1.5% Strain Amplitude Test

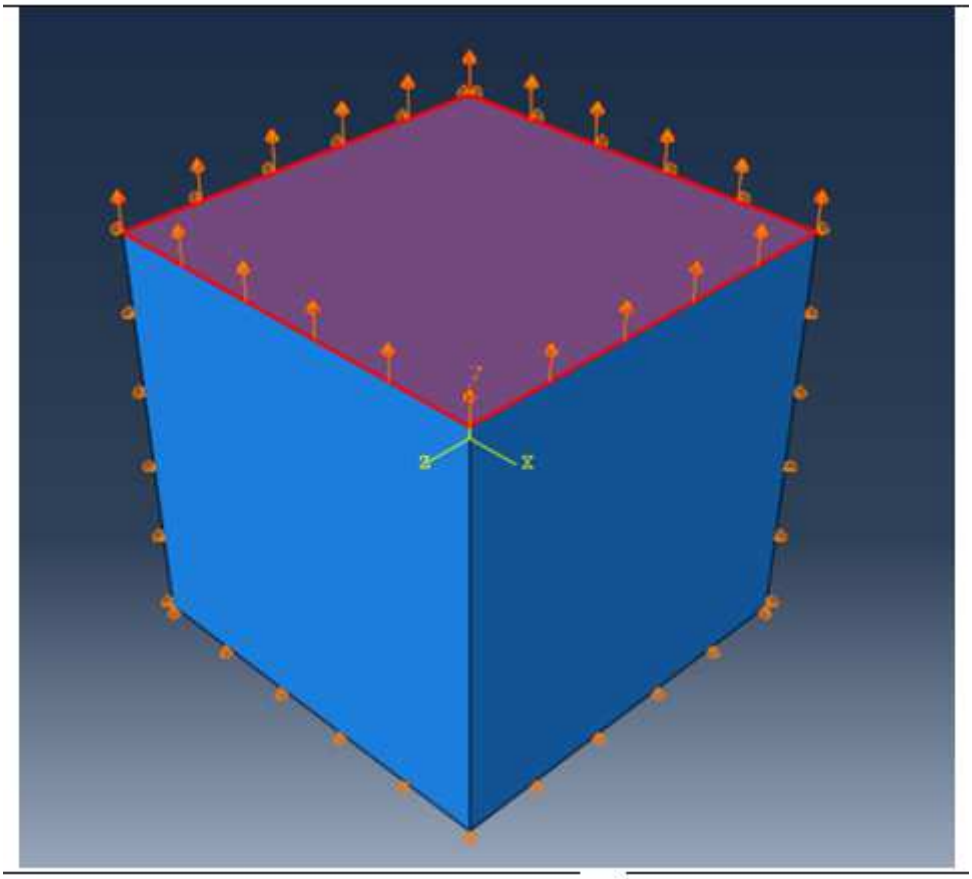

Figure 4

FEA Model for Material Model Validation

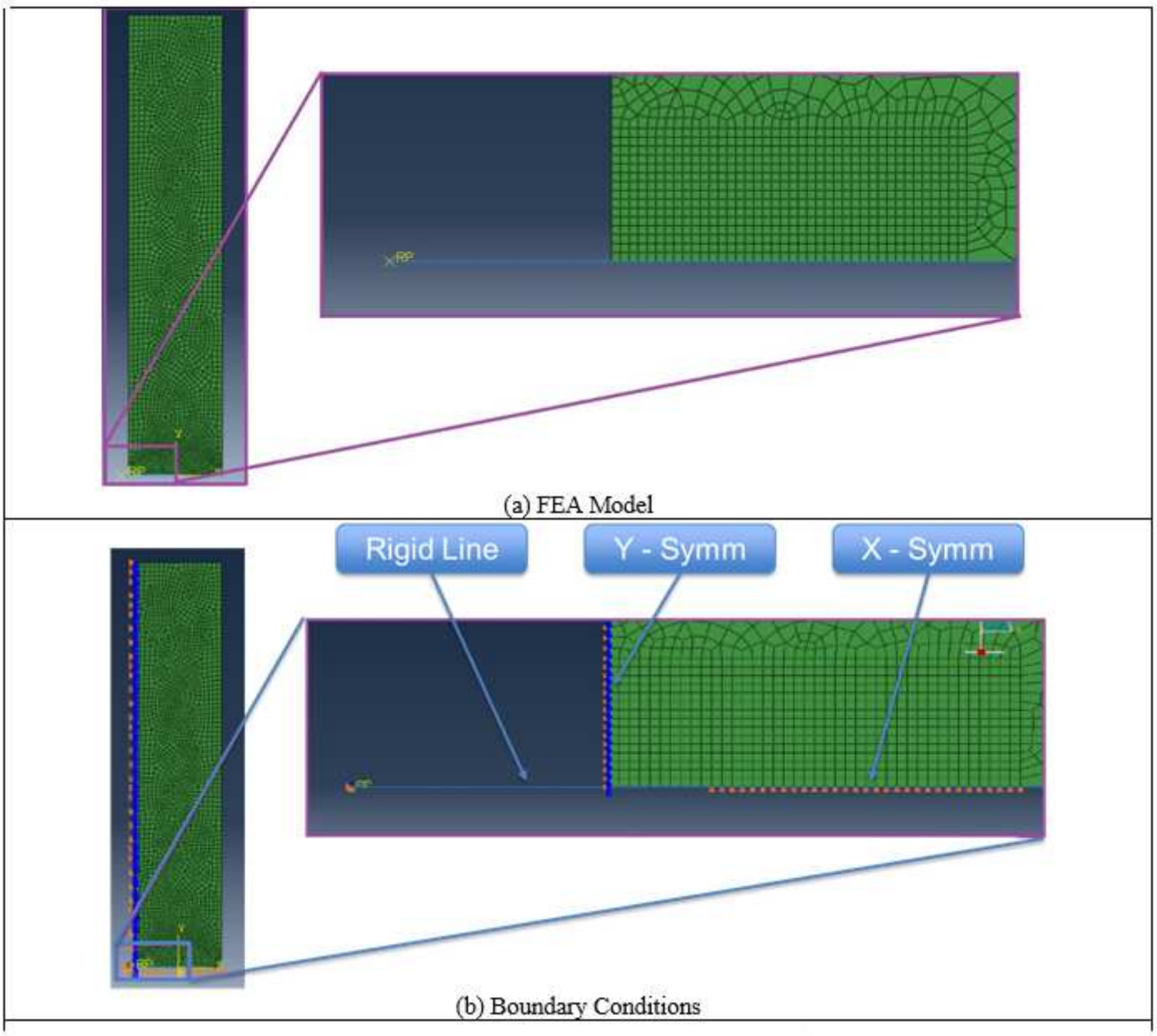

Figure 5

FEA Model for Fatigue Crack Simulation

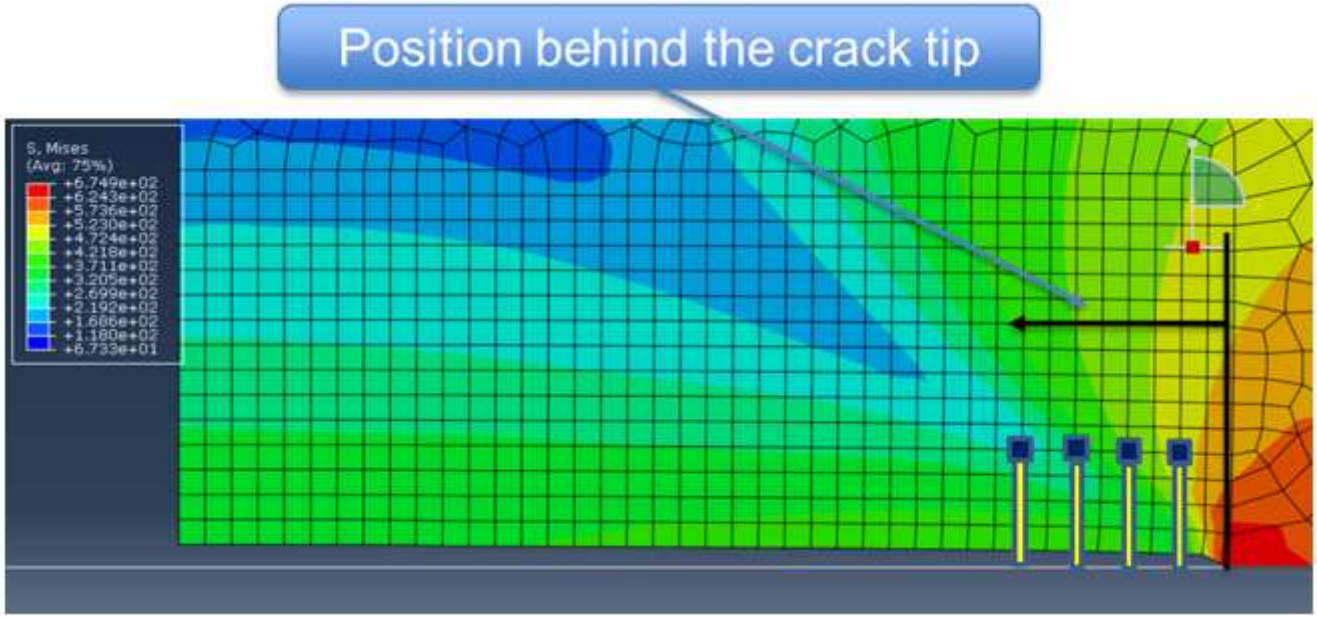

Figure 6

The positioning of the probe to obtain COD behind the Crack Tip

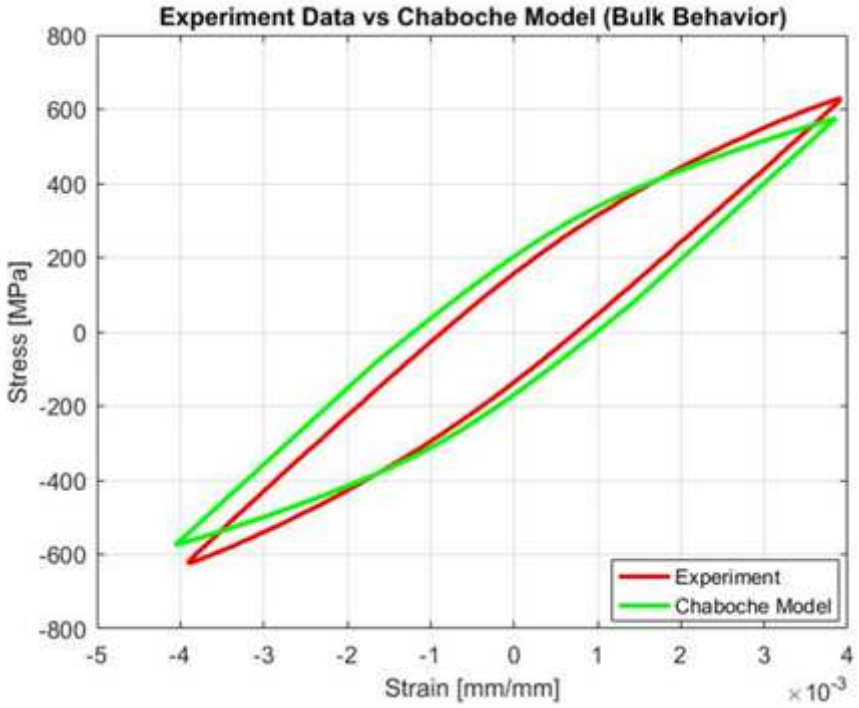

Figure 7

Bulk material behavior

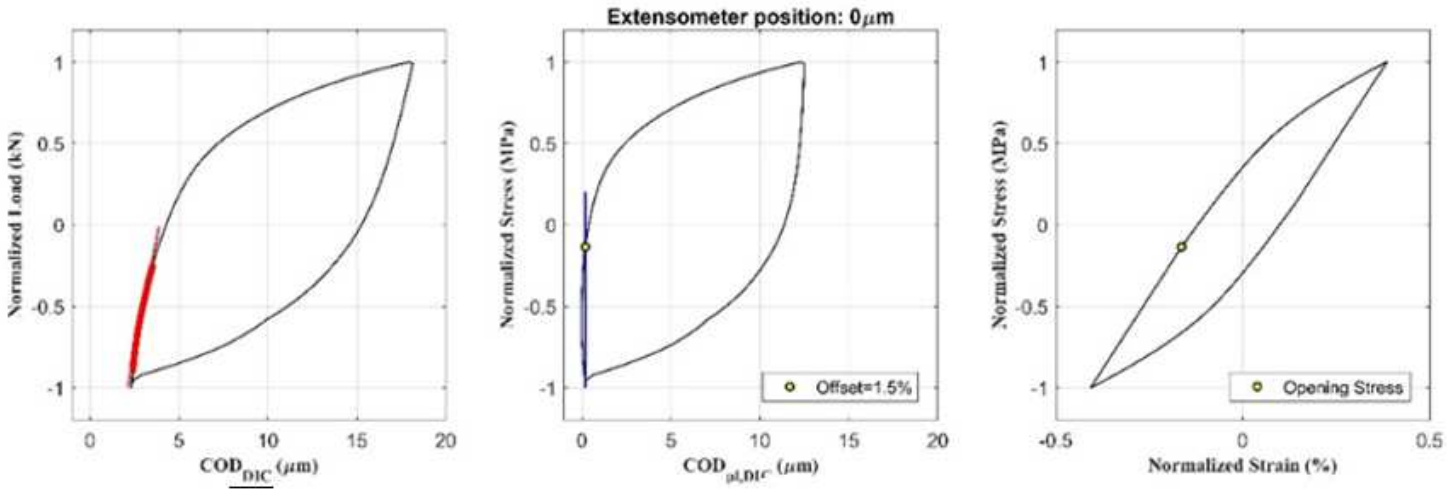

Figure 8

Determination of Opening Stresses (Crack 1600µm, 30NiCrMoV12, ΔƐ = 0.80%)

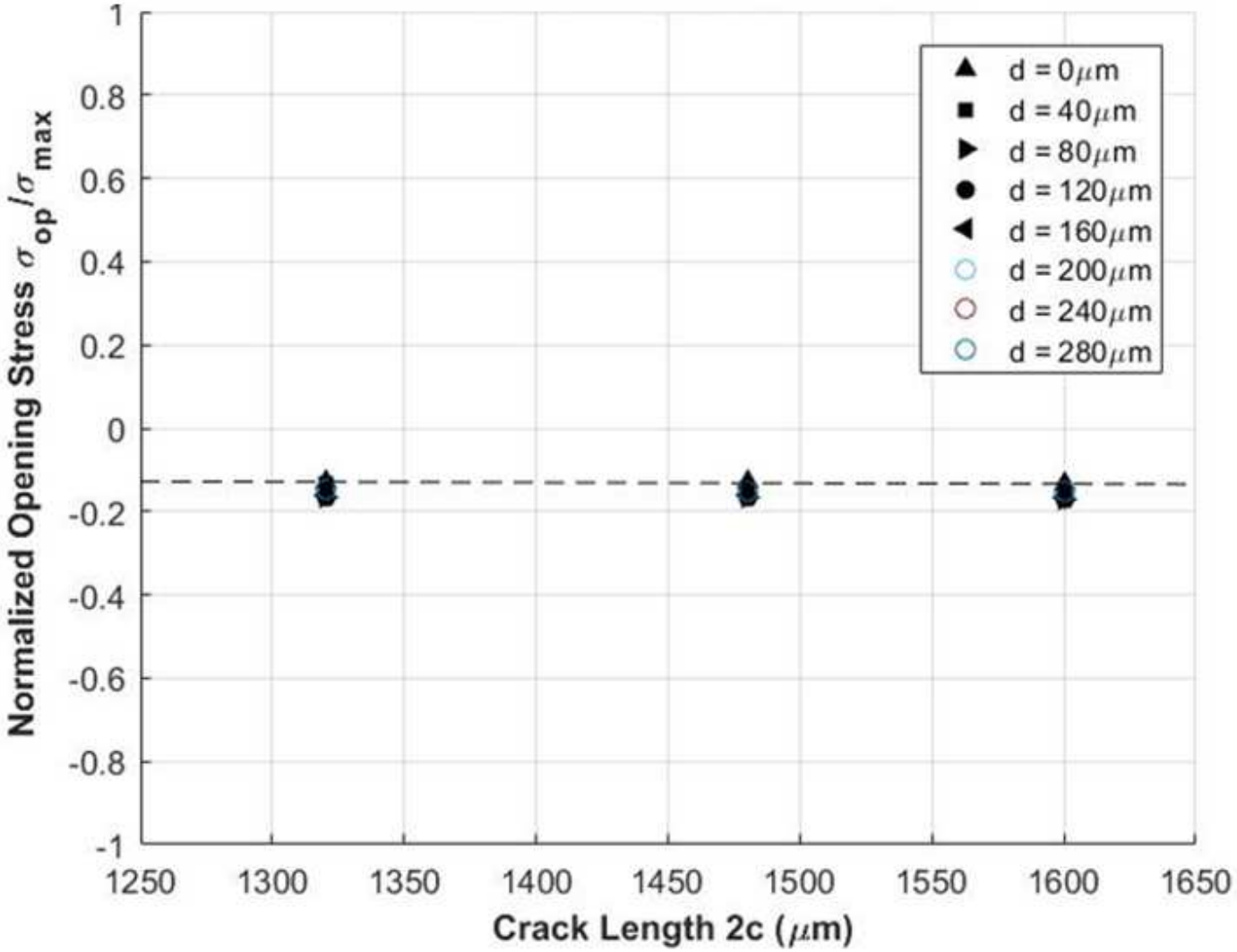

Figure 9

Crack Length vs Normalized Opening Stresses (FEM), 30NiCrMoV12, ΔƐ = 0.80%

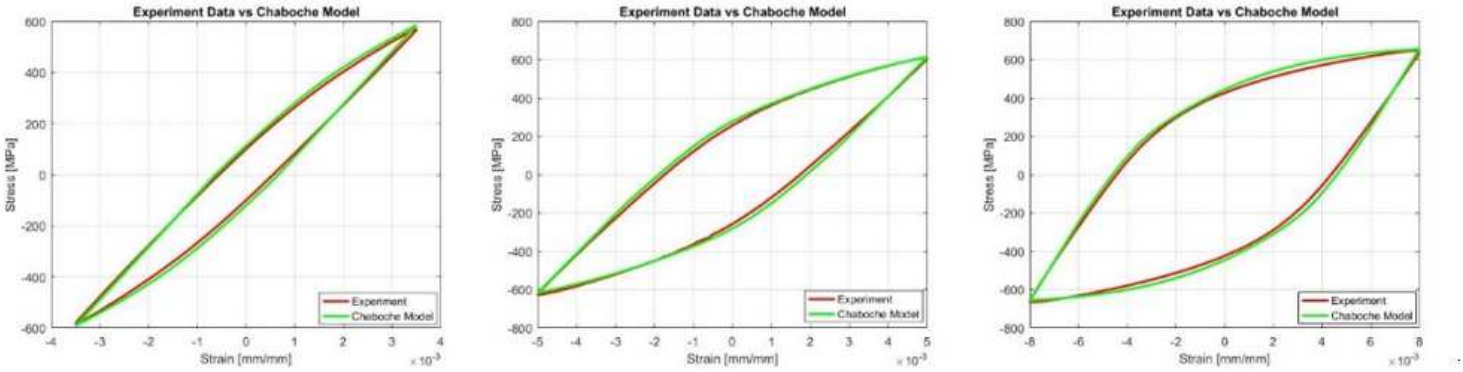

(a) 30NiCrMoV12

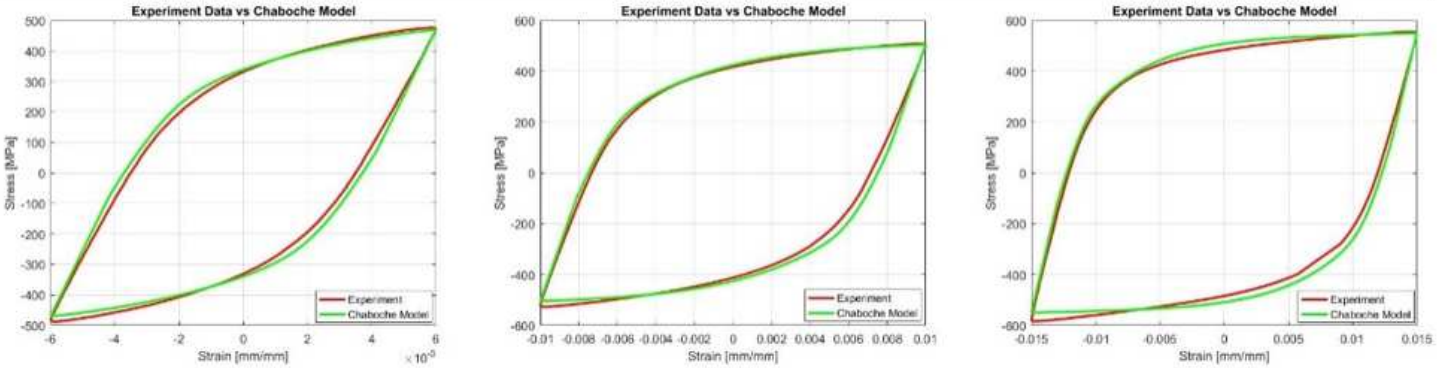

(b) 25CrMo4

Figure 10

Material Model vs. Experiments

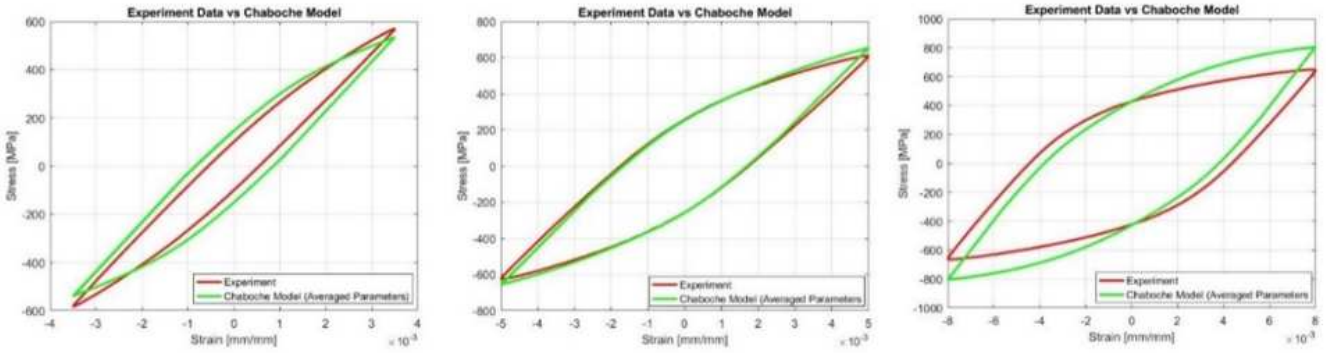

(a) 30NiCrMoV12

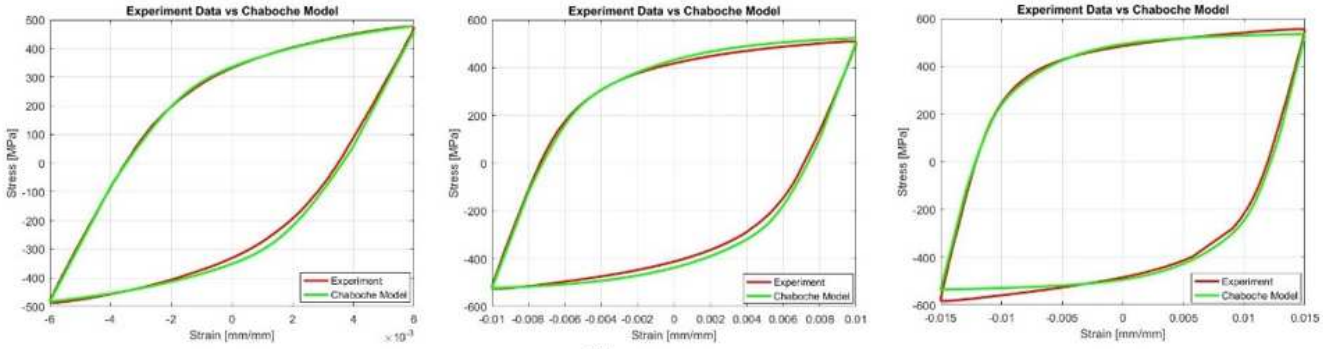

(b) 25CrMo4

Figure 11

Material Model (Averaged Parameters) vs. Experiments

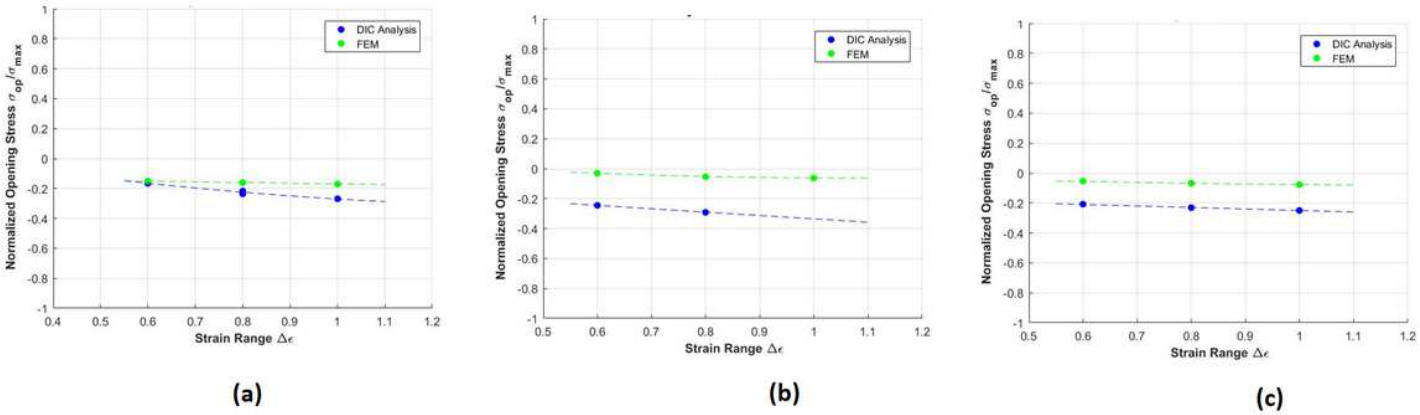

Figure 12

Opening Stresses Levels for different materials vs. Strain Ranges